On the effect of substrate oscillation onCrN coatings deposited by HiPIMS and dcMS

Monica Costa Rodrigues Guimaraes[a], Bruno César Noronha Marques de Castilho[a*], Carlos Cunha[a], Wagner Rafael Correr[a], Tamires de Souza Nossa[b], Fernando Alvarez[c], Jose Luis Garcia[d], Haroldo Cavalcanti Pinto[a]

[a] Escola de Engenharia de São Carlos – EESC, Universidade de São Paulo – USP, CEP: 13563-120, São Carlos - SP – Brasil

[b] Instituto Federal De Educação, Ciência E Tecnologia De São Paulo (IFSP), Departamento de Mecânica, 18202-000, Itapetininga, Brazil. e-mail: tamires.nossa@gmail.com

c IFGW-UNICAMP

d Sandvik Coromant

* *Corresponding author*

1 – Introduction

Different PVD techniques are currently studied due to the possibility of tailoring materials for a wide range of properties and deposit both mono and multilayers with different compositions and characteristics [1, 2]. Direct Current Magnetron Sputtering (DCMS) is a well-established deposition technique for metallic and compound coatings via reactive sputtering. On the other hand, High Power Impulse Magnetron Sputtering (HiPIMS) is a recently new technique being studied due to its capabilities to produce dense and hard coatings. It utilizes a pulsed current reaching higher ionization degree and higher peak power of the sputtered material when compared to DCMS hence increasing coating density and hardness [3, 4].

Nitrides, carbides and/or carbonitrides for tribological applications are investigated due to its chemical stability, high hardness and wear resistance [5]. Amongst them, chromium nitrides attracts interest because it can replace titanium nitrides in high temperature applications and present high corrosion and oxidation resistance combined with low friction coefficient [6 – 9] . Due to its lower residual stress, it is possible to produce thicker coatings than the average coatings produced by PVD [9].

The use of multilayers is described to effectively reduce crack propagation, increase hardness and wear resistance. The different layers serve as a path to deflect the crack thus avoiding the full delamination of the coating [1]. Although multilayers are currently developed by changing the chemical composition of each layer, there is no study in literature about multilayers and periodicity observed of the same material formed due to orientation growth.

In this study, we propose a new way to produce multilayer coating by using a pilot plant PVD deposition chamber and oscillating the substrate facing the target therefore modifying coating orientation.

2 – Experimental Details

2.1 – Deposition parameters

Chromium nitride coatings were deposited by HiPIMS and unbalanced magnetron sputtering on AISI 304L stainless steel. All substrates were grinded, polished to a mirror finish with colloidal silica and then ultrasonically cleaned in acetone.

The coating depositions used a Plasma HiPIMS 250 (Plasma LIITS, Brazil) chamber equipped with a 220 x 110mm Cr target with 99.5% purity. A pressure of 2 mtorr and a temperature of 400 °C was used throughout the deposition process. The substrates were bombarded with Cr+ ions as a final cleaning process (ion etching) to remove impurities from the surface and to provide ion implantation, as a mean to improve adhesion. Furthermore, a base layer of chromium was deposited to improve the adhesion of the coating. Throughout the deposition process the N_2 and the Ar flow rates were 50 and 40 sccm respectively.

The power was set at 900W and bias was varied from 0, -20, -40, -60, -100 and -140V for both DC and HiPIMS deposition. HiPIMS pulsed frequency was set to 400, 450 and 500Hz. More importantly, during the deposition an oscillation of 5° in 120 seconds was imposed to the substrate to produce the multilayer structure.

2.2 – Mechanical Characterization

A PB1000 Mechanical Tester (Nanovea, USA) with a Berkovich tip was used for nanohardness instrumented test. The measurements were performed with a 30 mN maximum load and 60 mN/min load/unload rate. For each sample, 15 measurements were made and then averaged, all with penetration depth lower than 10% of coating thickness to make sure no substrate influence was observed.

2.3 – Structural and Morphology Characterization

Two difractometers were used to provide structural information on the coatings. In a first moment, theta-2theta diffractograms were made using a diffractometer Rigaku Rotaflex - Ru200B with monochromatized CuKα radiation, for phase and texture coefficient determination.

Texture coefficients $T_{(hkl)}$ of (111), (200), (220) and (311) reflections were determined from the intensities of the CrN peaks. In general, the $T_{(hkl)}$ for any reflection can be determined using the following relation

$$T_{(hkl)} = \frac{I_{hkl}^{m}}{I_{hkl}^{ICDD}} \frac{\sum_{hkl} I_{hkl}^{ICDD}}{\sum_{hkl} I_{hkl}^{m}}$$

where I_{hkl}^{m} is the measured relative intensity of a plane (*hkl*), I_{hkl}^{ICDD} is the standard intensity of the plane (*hkl*) taken from the ICDD data (card no. 00-001-0065).

The Si powdered sample was used as the crystalline standard in order to make corrections due to the instrumental broadening of diffraction lines. The XRD line-broadening analysis was performed with the analytic function method, with Cauchy or Gaussian distributions. The Kα_2 component was removed by the method of Rachinger after background subtraction. The crystallite size (D) and microstrain were determined by

$$D = k\lambda/\left(\beta_C^f cos\theta\right), \varepsilon = \frac{1}{4}\beta_G^f cot\theta$$

where the factor k is related to the ratio between the integral widths of Cauchy (β_C^f) and Gauss (β_G^f) functions, λ is the wavelength of the X-ray radiation and θ the Bragg angle.

Another diffractometer, a MRD-XL Diffractometer (PANalytical, the Netherlands) with Mo anode (Kα – 0.7093) was used to study residual stresses of the coatings with the $\sin^2\psi$ method. The analyzed peaks were (422); (511) and (333) for CrN and (222) for Cr due to higher multiplicity and increased resolution. Furthermore, 7 points of psi were used, with $\sin^2\psi$ varying from 0 to 0.9 with increments of 0.15.

Top and cross-sectional images of the coating for morphology observation and thickness measurement were made by using Field Emission Scanning Electron Microscopy (FEI, The Netherlands). The determination of chemical composition was made by Energy Dispersive X-Ray Spectroscopy (Apollo X SDD, EDAX, USA) attached to the SEM. Finally, the roughness was calculated by Atomic Force Microscope Nanosurf Flex (Nanosurf, Switzerland) on a 30 x 30μm area.2.4 – Electrochemical Characterization

To this analysis were sectioned the samples that showed a better result previously on mechanical characterization and just only one sample of each method was submitted to electrochemical characterization: the CrN films of DC (bias of -140 V) and the HiPIMS produced at 400Hz (bias -60 V). The samples CrN coating surfaces were polished with diamond paste 1 μm to ensure a surface roughness pattern. The Electrochemical test was performed on the Potentiostat Galvanostat PerkinElmer VersaSTAT4 at room temperature on sample exposed area of 0.2 cm² in a solution of 3.5% p/p NaCl. The Corrosion Open Circuit were obtained using a reference electrode of

Ag,AgCl (0.197 V) and a solid working electrode. The Tafel curves or polarization resistance parameters used were potential range of -0.25 V to 0.25 V and a scan rate of 0.167 mV/s.

3 – Results and Discussion

3.1 – Chemical composition

The chemical composition of the coating was evaluated by EDX. All the coatings presented stoichiometric composition with (49±2) at% N and (51±2) at% Cr which indicates a good adjustment of the deposition parameters (Ar and N_2 flow).

3.2 – Structural evaluation

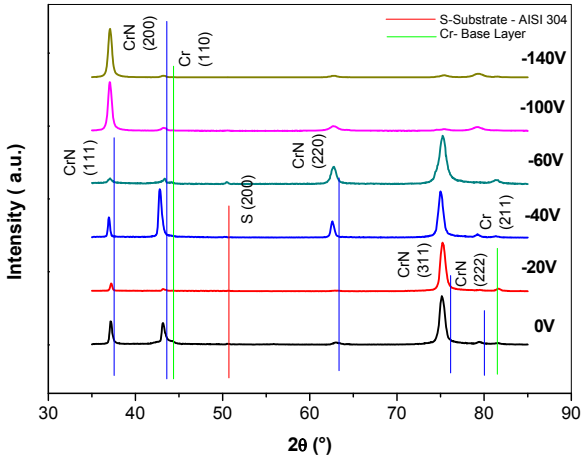

Figure 1: XRD patterns from all DC deposited coatings. All coatings present a shift to the left on 2θ values, indicating presence of residual stress.

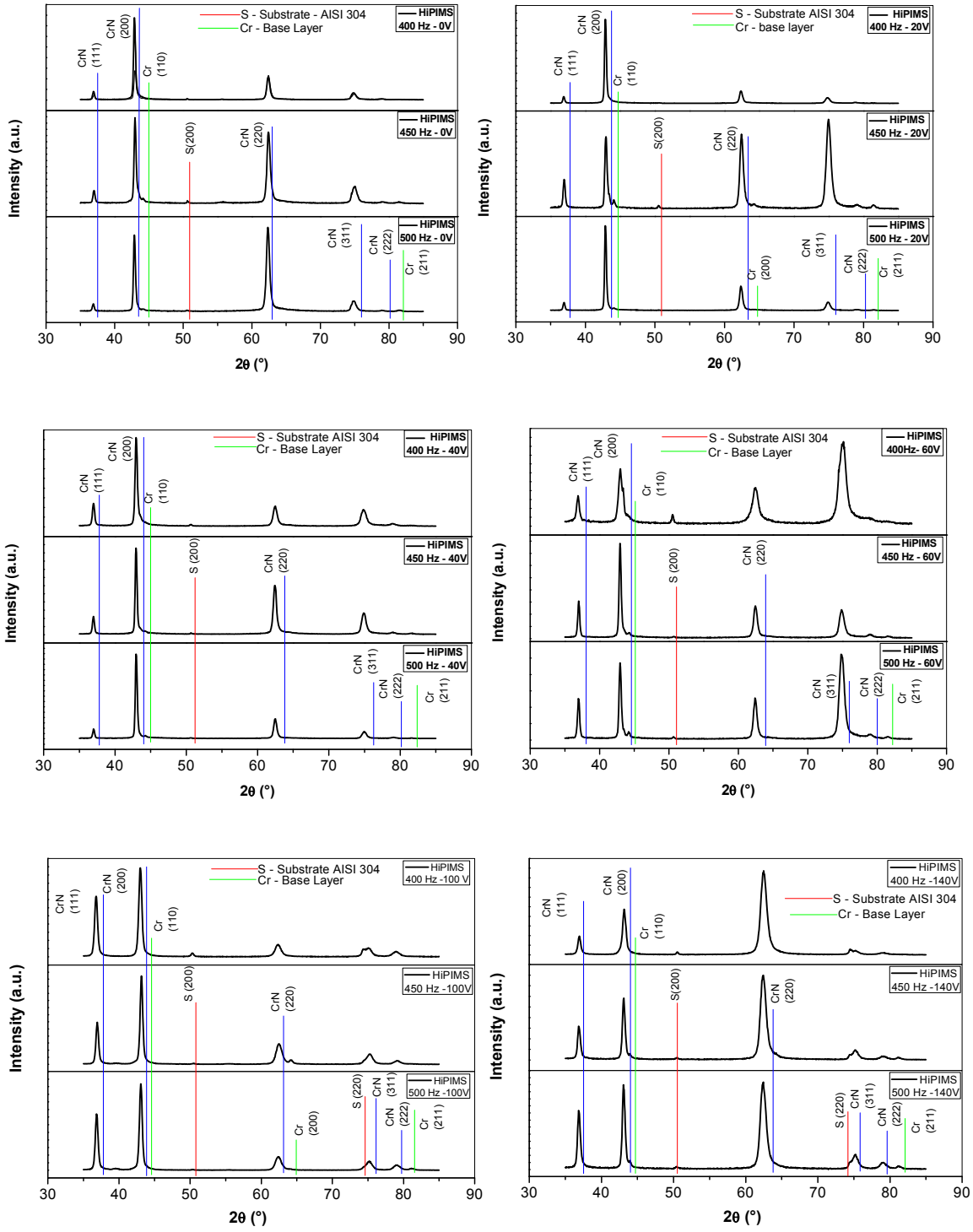

Figure 2: XRD patterns from all HiPIMS deposited coatings. The shift to the left indicates presence of compressive residual stress.

The diffractograms of Figure 1 and 2 confirms for all DC and HiPIMS coatings the presence of CrN face centered cubic phase. All CrN peaks were shifted to the left towards lower 2θ values, which indicates the presence of compressive residual stresses on the xy plane of the sample causing an expansion on the z direction due to Poisson expansion. Therefore, these residual stresses were further evaluated in this paper. The thickness of the coatings (6-8µm) combined with the penetration of the Cu radiation in this material are the reason why some signal from the base layer and the substrate were found in XRD results.

The presence of texture on CrN coatings was evaluated by XRD patterns as can be observed in Figure 3.

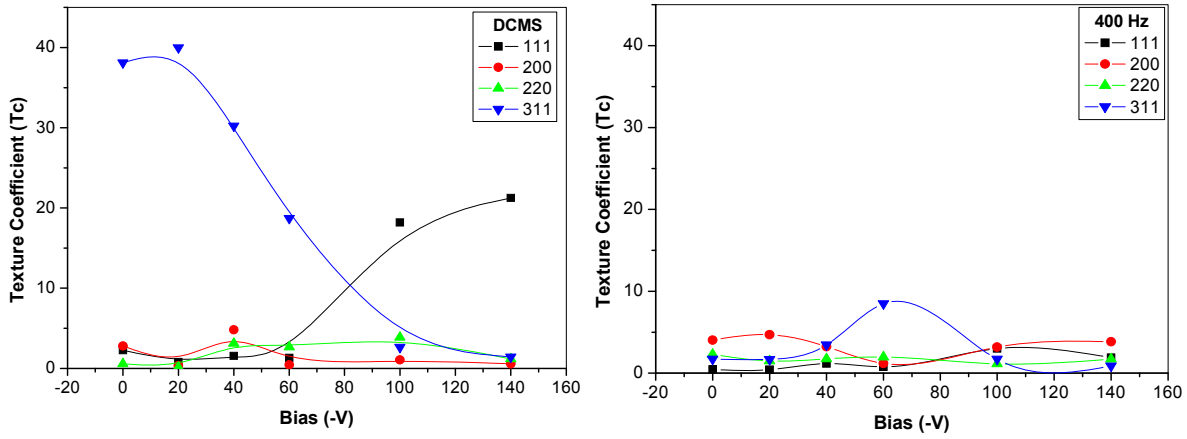

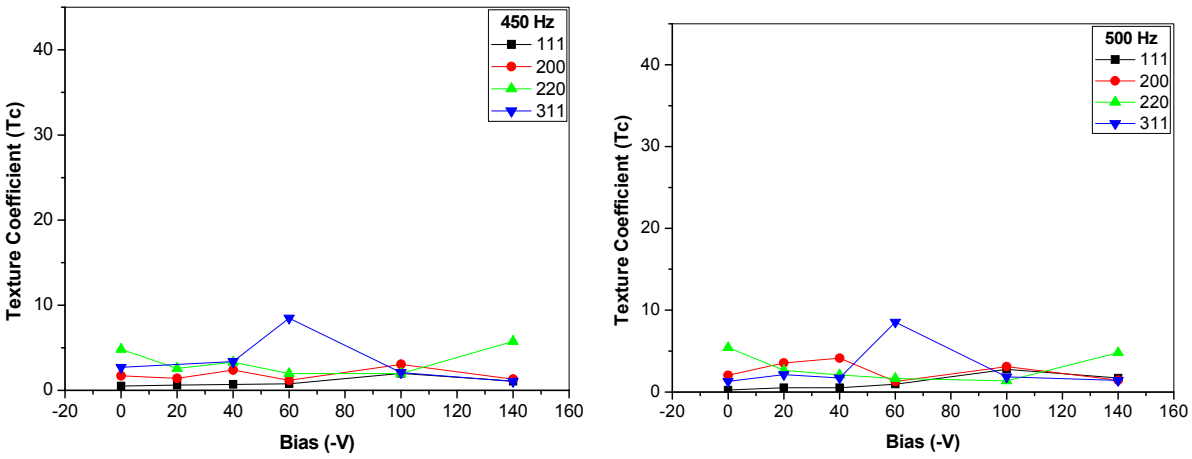

Figure 3: Texture coefficient of all deposited coatings. For all HiPIMS frequencies a preferential orientation growth on (311) plane was found for -60V bias.

The DC coatings presented a change of preferential orientation as the polarization changed. Preferential orientation changed from (311) to (111) plane as the polarization changed from lower bias (0, -20, -40 and -60V) to higher bias (-100 and -140V).

The correlation between process condition and texture can be described either by thermodynamic or kinetic growth models. The polarization tension affects the coating preferential orientation due to the interaction of different driving phenomena such as surface energy, atoms mobility and ion bombardment [10]. As the polarization is increased, the mobility of the surface atoms is also increased, which results in a transition of the diffusion of atoms among planes to a diffusion among grains [11].

Chromium nitride has a FCC structure, thus the plane with higher atom density is the (111), which has less surface energy [12]. For coatings deposited without bias, the (311) plane has higher texture coefficient which is the plane with higher surface energy when compared to the (111). Therefore,

the change observed on the texture for DC coatings can be explained by the increased mobility of the atoms contributing to a different mechanism of diffusion.

For HiPIMS coatings the influence of the frequency and bias on the preferential orientation growth was also evaluated. Regardless of the frequency, higher texture coefficient was found on (311) plane for -60V.

According to [13], lower duty cycles provide higher current peak, therefore leading to a more intense ion bombardment and to a more pronounced texture. This effect could not be observed in our study probably due to the small interval of frequency (400 – 500Hz).

The preferential orientation growth is determined by the least total energy resulting from the competition between strain and surface energy. According to [14], if the surface energy is dominant, cubic nitrides grow with texture on (200), which has smaller surface energy. If the strain energy is dominant, then the texture will be on (111) plane. The intensity of the surface energy is higher for the (311) plane, followed by (111), (110) and (100). Nouveau [15] showed that the presence of the plane (311) was related to the different growth rate between the planes (111) and (311) and for the preferential resputtering on the (111) plane.

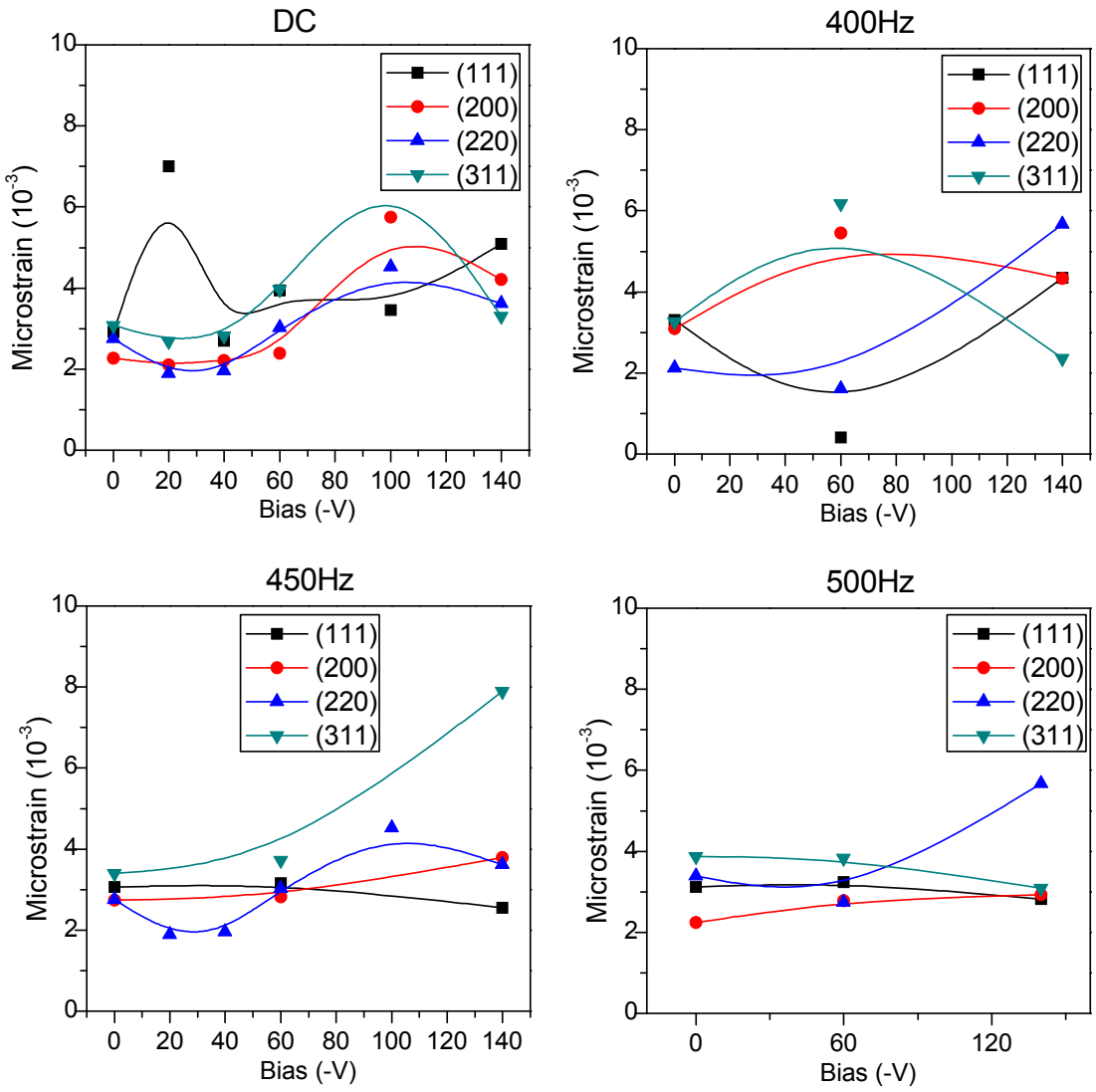

Figure 4: Results of microstrain for all coatings.

The microstrain behavior for all coatings can be observed in Figure 4. As the bias was increased so was the ion bombardment, therefore inducing the formation of more lattice defects and thus increasing in general the microstrain.

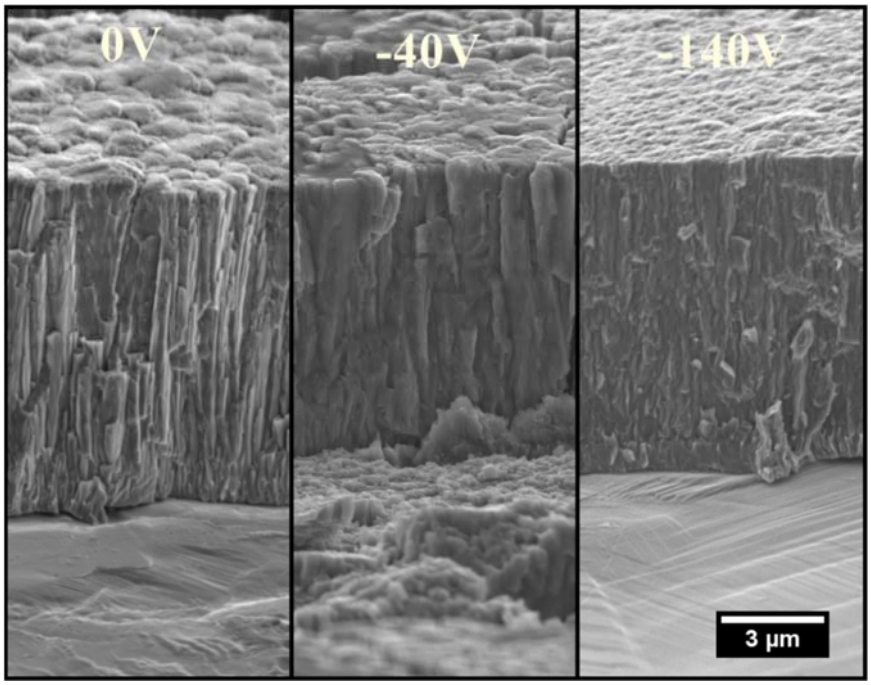

Figure 5: SEM fracture images of DC coatings. The coatings exhibit columnar growth for low or no bias which evolves to a dense structure for higher values of bias.

The SEM images were used to calculate deposition rate for all DCMS coatings. No significant influence of bias was noted and the deposition rate was around 3.9µm/hr. It is also possible to verify the validity of the zone model proposed by Anders [16]. As the bias was increased, so was the energy of the atoms arriving to the surface of the coating. This is reflected on the mobility of these atoms, providing densification of the coating and the reduction of the size of the columnar structure (from 0V to -40V). With a further increase of energy, it is not possible to discern the columnar structure and a featureless coating is observed (-140V). This morphology change is due to a higher ion flux. As the bias was increased, higher mobility is given to the atoms, which in turn will fill the voids between grains and break the columnar grow, thus creating new nucleating sites [17-18]. Therefore, we moved from Zone 1 to Zone T in the diagram without the decrease of thickness observed for higher applied energies.

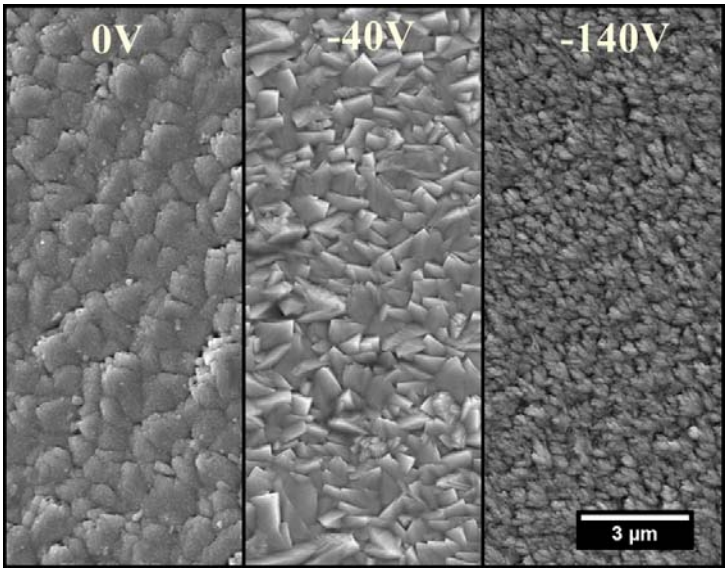

Figure 6: Microstructure evolution of DC coatings. The grain size is reduced when increasing bias voltage.

Figure 6 shows the microstructure evolution of the coatings and confirms the analysis made for the fracture image. It is possible to observe how grain size is reduced due to the increased bias.

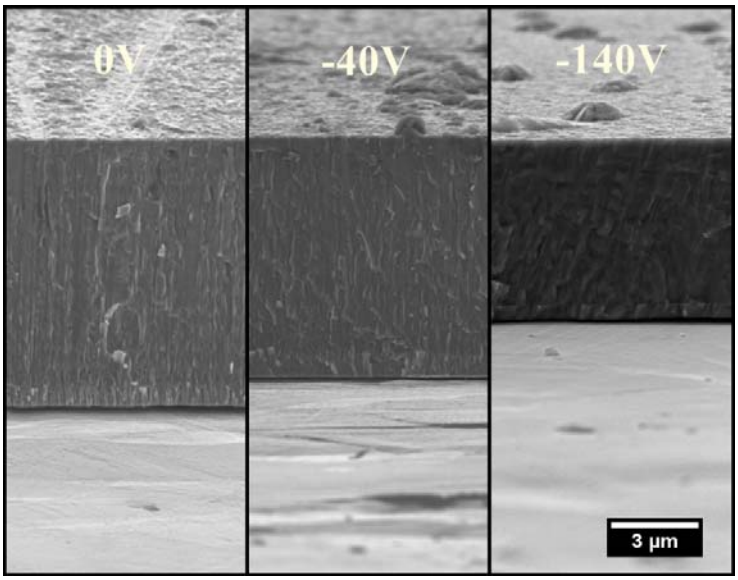

Figure 7: SEM images of HiPIMS coating. The reduction of the deposition rate due to bias increment is observed. The columnar aspect of DC is not observed for any bias value.

Differently of the independence between bias and deposition rate observed for DC deposited coatings, HiPIMS coatings presented reduction of deposition rate as the bias was increased. It is possible to observe from Figure 7 that, for the same frequency (450Hz) the total thickness of the coating was reduced from 8.4µm to 5.6µm. The reduction in coating thickness is related to the densification of the coating due to the higher energy of the arriving atoms. Another concurrent phenomenon is the re-sputtering, which also contributes to a reduction on deposition rate of the material. The peak power of HiPIMS sources are higher than the one for DC, which means more energy is given to the ions. This is also explained by the SZM proposed by Anders, in which higher energy promotes the reduction of the deposition rate. This was also observed by [19] in a study on stress for TiN films deposited by HiPIMS. No significant changes in coating morphology as a function of frequency was observed neither for top nor cross-section images and therefore these images are not presented here.

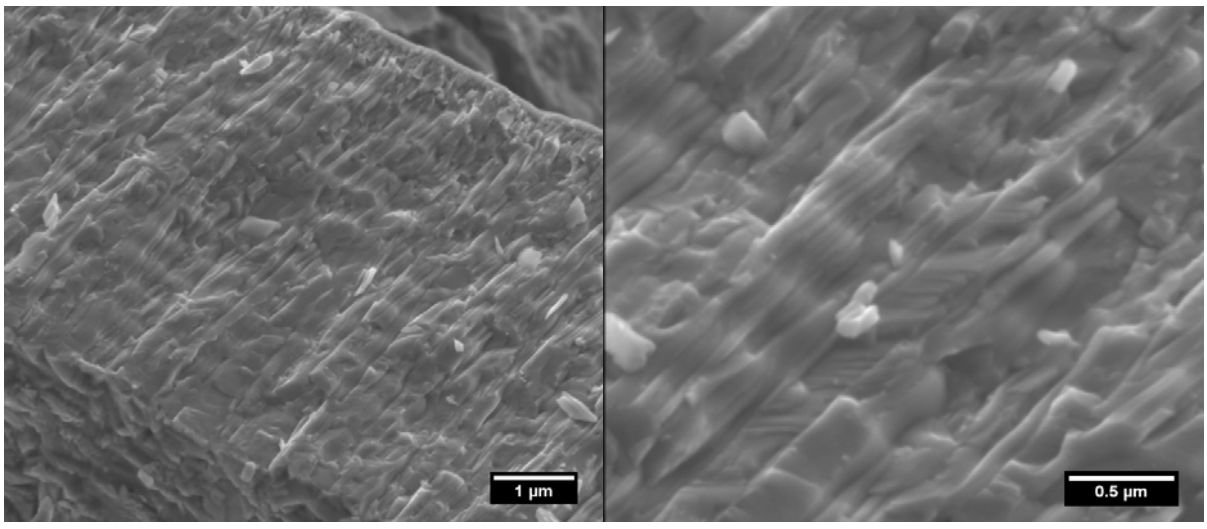

Figure 8: Evidence of multilayer periodicity due to orientation growth.

The modulation phenomena proposed in this paper can be observed with more detail in Figure 8. The observed periodicity of 0.4 to 0.5μm corresponds to the oscillation period of the substrate facing the target.

Information on crystallite size was extracted from the XRD data. The calculated values of crystallite size decreases with the increment of bias as shown in Figure 9. These calculations agree with the SEM top and cross-sectional images, which further contributes to the interpretation of a reduction of the columnar feature for lower bias and a trend to form nanocrystalline grains for higher bias voltage.

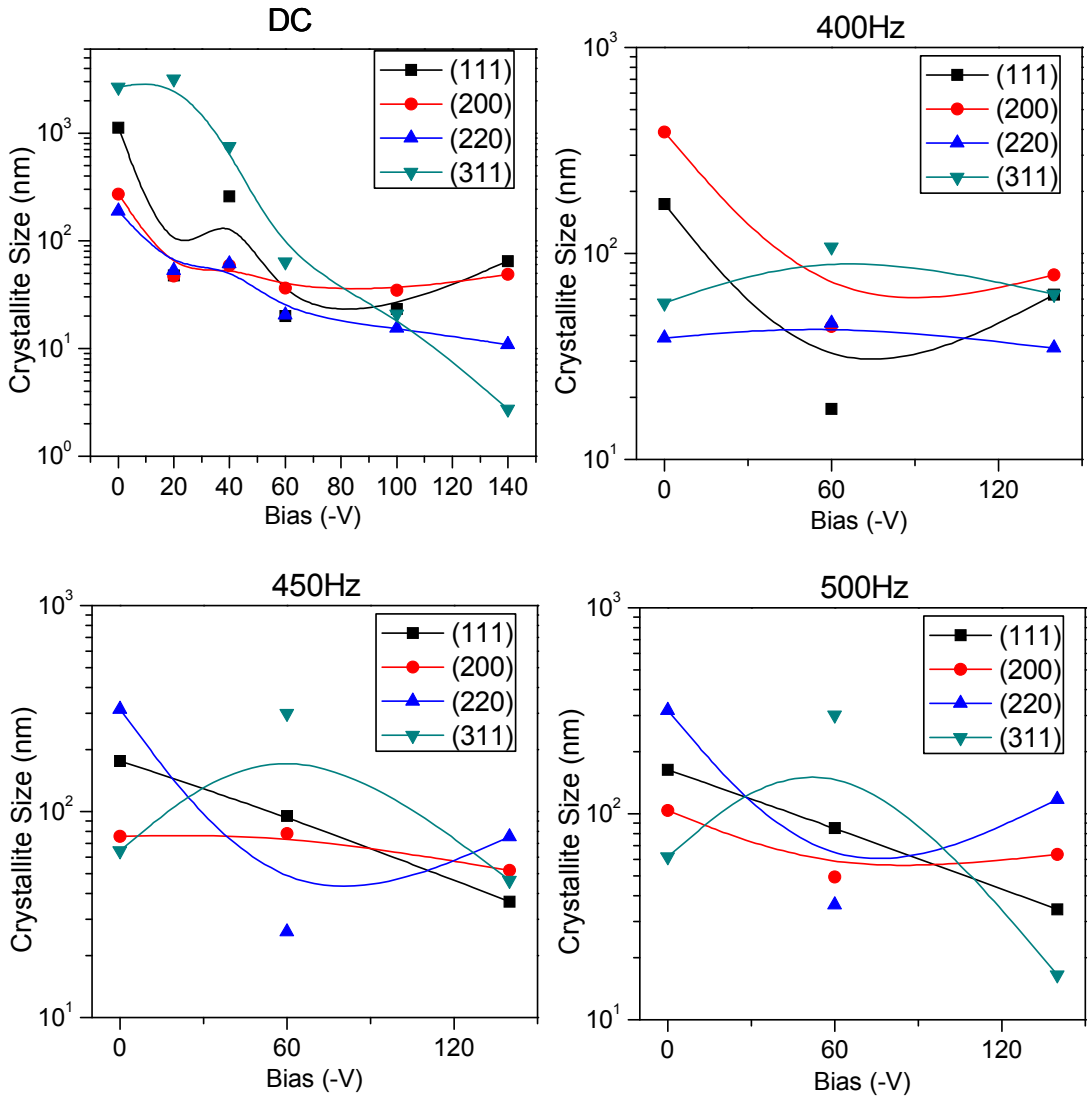

Figure 9: Crystallite size calculated by XRD data. The reduction of crystallite size as the bias is increased confirms the analysis and discussion of the SEM images.

The AFM measurement of those coatings show that the change in bias influences roughness. The mean roughness changed from 78.5 to 35.2nm with the change of bias from 0 to -140V respectively. However, the minimum roughness value was found at -100V bias, 30.2nm. The reduction on crystallite size also affects the coating surface roughness. For DC coatings it is observed a general reduction of the coating roughness (Ra) as the bias is increased, which is also

observed for crystallite size in all planes. HiPIMS coatings present invariant roughness for lower bias but for higher values of bias there is a higher number of cone like defects due to higher energy, which in turn affect the measurement of roughness.

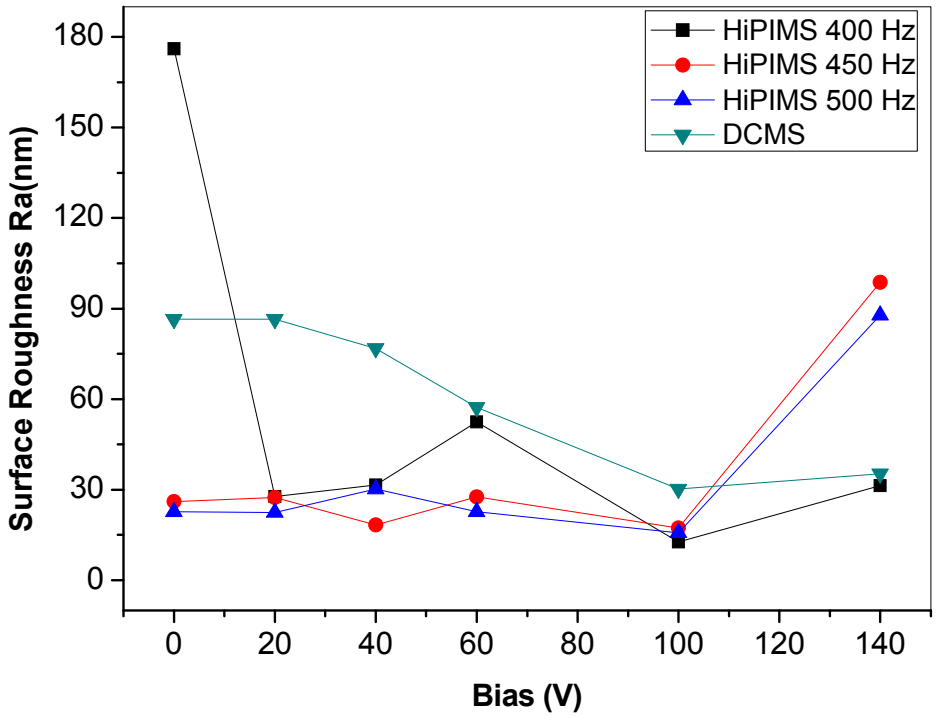

Figure 10: Surface roughness as a function of bias voltage.

3.3 - Residual Stresses

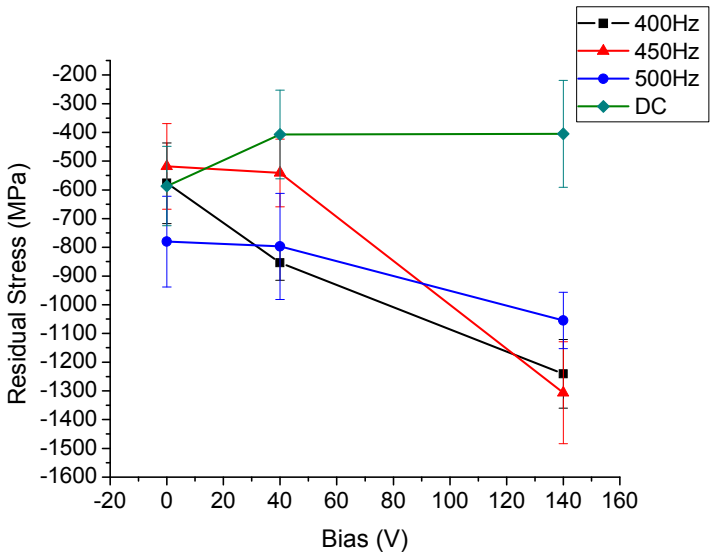

Figure 11: Residual stress as a function of bias. Compressive stress found for all the investigated range. Higher stress as the bias was increased from 0 to 140V.

The residual stress analysis shows an increase in the compressive stress for higher values of bias for HiPIMS deposition. The higher peak power of HiPIMS source combined with the presence of higher bias raised the ion flux and provided more compaction of the coatings, therefore contributing to higher residual stresses.

3.4 - Hardness

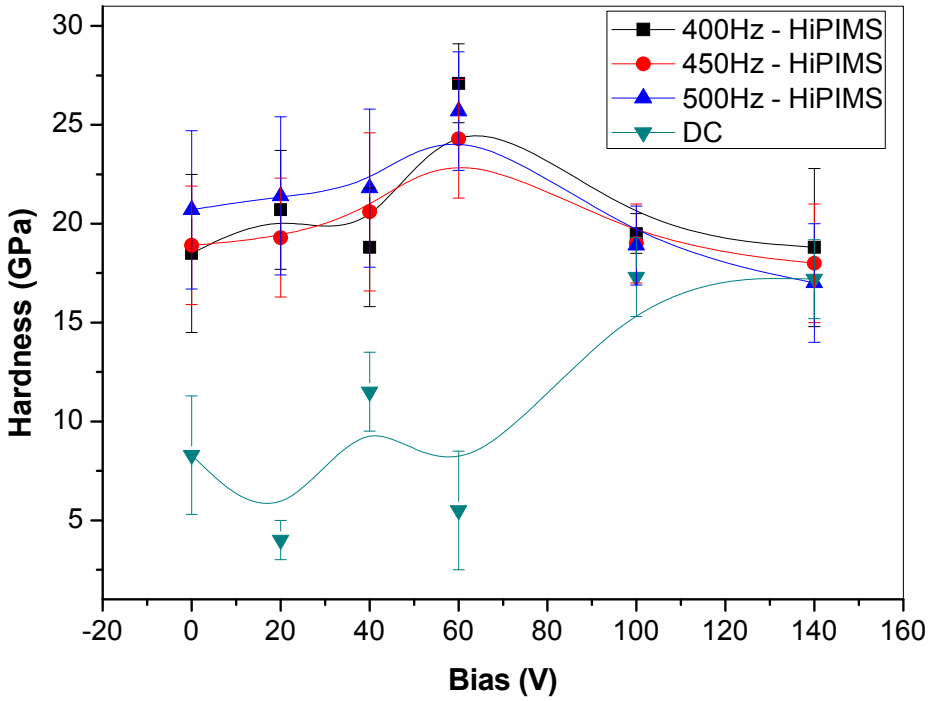

Hardness results presented similar behavior of the morphology, which means that no significant difference was found with changing the frequency, at least for the investigated range. The higher achieved value of hardness was at 60V bias at 400Hz, 27.1GPa. DC coatings had a different behavior: It presents two distinguished regions, one for bias lower than 60V, in which low values of hardness were found, oscillating around 7GPa. The other region, for bias higher than 60V, higher values of hardness were achieved, with peak value of 17.3GPa for 100V. Inside both regions hardness is independent of the applied bias.

3.5 – Electrochemical Behavior

On general, CrN coatings have an excellent corrosion resistance due its dense microstructure and a surface passive layer [20, 21] formation. This can be seen on Figure 13 that shows polarization

curves of potential (mV) versus current density (A/cm²) to surfaces of CrN films produced by DC (-140 V) and HiPIMS (400 Hz, -60 V).

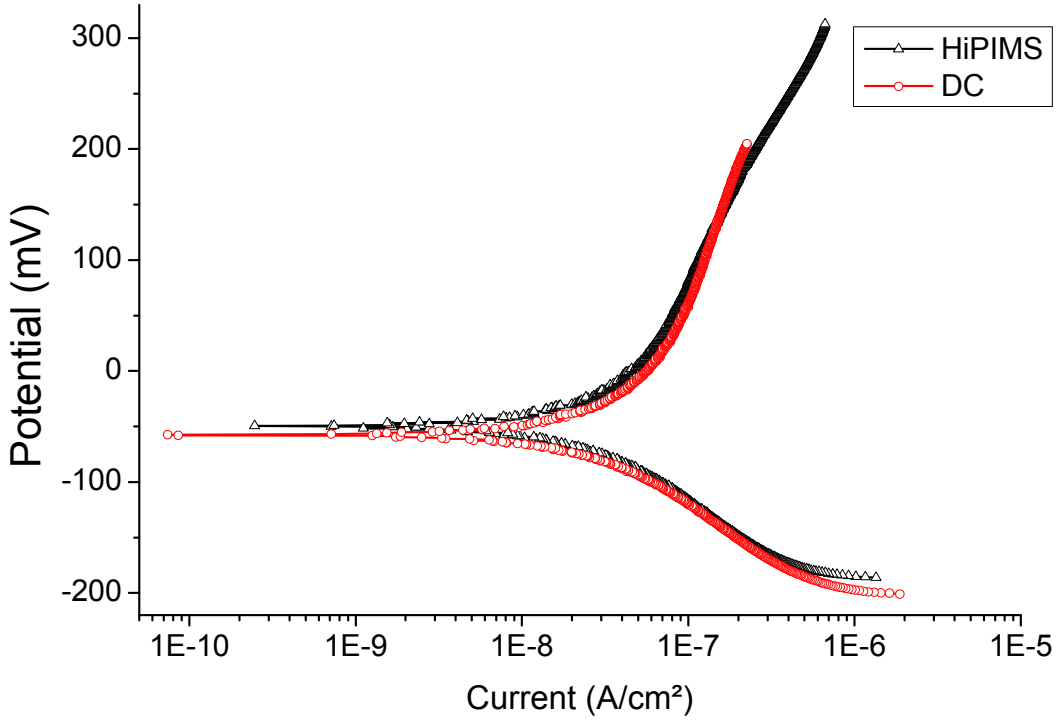

Figure 13. Polarization curves for the CrN films surfaces deposited by DC (-140 V) and HiPIMS (400 Hz, -60 V).

Both samples showed a high corrosion resistance, the corrosion potentials (E_{cor}) and the current densities (I_{cor}) derived by polarization curves using Tafel plots, were subtly different to DC and HiPIMS samples. The CrN coating deposited by DC showed a more positive E_{cor} of -52.273 mV and a small I_{cor} of 3.56 (10-8 A/cm²) while the HiPIMS sample presented an E_{cor} of -58.844 mV and I_{cor} of 4.68 (10-8 A/cm²). The CrN coating produced with DC presented a corrosion resistance slightly higher than produced by HiPIMS, this difference can be attributed to reduction in crystallite size of 100 nm (HiPIMS 400Hz -140V) to 70 nm (DC -60V). In addition, this difference

can be too attributed to the compressive residual stresses when high stresses levels can generate a decrease in corrosion resistance [22-24].

4 – Conclusions

In this work we presented for the first time a new feature formed in both DCMS and HiPIMS due to the oscillation of the substrate facing the Cr target. It was observed a multilayer structure with the same period of the oscillation and related to the change of the orientation during the deposition process. CrN coatings with elevated hardness (27 GPa) were produced and the influence of bias and frequency were investigated with XRD, SEM images and AFM. Preferential orientation growth on (311) plane for -60V might be related to the development of harder coatings at this bias level. HiPIMS showed higher hardness and lower surface roughness than DCMS throughout the investigated range of bias, but no significant influence of HiPIMS pulsed frequency could be verified. Both CrN coatings produced by HiPIMS and dcMS showed comparable corrosion resistance.

Acknowledgements

The Authors would like to thank MAHLE Metal Leve and BNDES (Decision Dir. 640/2012) for funding. MCRG, BCNMC and PRTA acknowledge the Brazilian agencies CAPES and CNPq for the scholarships. The authors would like to thank Carlos Cunha for operating the deposition chamber. Furthermore, the Authors would like to thank Wagner Correr, from the Sao Carlos Institute of Physics, University of Sao Paulo, for all the help with images, discussions and equipments. HP is a CNPq fellow. This work was supported by the CREATE-Network Project, Horizon 2020 Program of the European Commission (RISE Project No 644013). H. Pinto and J. Garcia thanks the financial support of the project Create-Net Project N° 318903 financed by the EU.

References

[1] HOLMBERG, K.; MATTHEWS, A. Coatings Tribology: Properties, Mechanisms, Techniques and Applications in Surface Engineering. London: Elsevier Science, 2009.

[2] BIRKHOLZ, M. Thin Film Analysis by X-Ray Scattering. Weinheim: WILEY-VCH Verlag GmbH & Co. KGaA, 2006.

[3] HASHMI, S. *et al.* Comprehensive Materials Processing. Amsterdam: Elsevier, 2014.

[4] BUNSHAH, R. F. Handbook of Hard Coatings - Deposition Technologies, Properties and Applications. New York: Noyes Publications, 2001.

[5] MAISSEL, L. I.; GLANG, R. Handbook of Thin Film Technology. New York: McGraw-Hill Handbooks, 1970.

[6] Milosev, I.; Strehblow, H.H.; Navinsek, B. XPS in the study of high-temperature oxidation of CrN and TiN hard coatings. Surface & Coatings Technology, v. 74-75, p.897-902, 1995.

[7] BARSHILIA, H. C. et al. A comparative study of reactive direct current magnetron sputtered CrAlN and CrN coatings. Surface & Coatings Technology, v. 201, n. 6, p. 2193-2201, Dec 4 2006. ISSN 0257-8972.

[8] EHIASARIAN, A. P. et al. High power pulsed magnetron sputtered CrNx films. Surface & Coatings Technology, v. 163, p. 267-272, Jan 30 2003. ISSN 0257-8972.

[9] NAVINSEK, B.; PANJAN, P.; MILOSEV, I. Industrial applications of CrN (PVD) coatings, deposited at high and low temperatures. Surface & Coatings Technology, v. 97, n. 1-3, p. 182-191, Dec 1997. ISSN 0257-8972.

[10] ZHANG, T. F. et al. Influence of negative bias voltage and deposition temperature on microstructure and properties of superhard TiB2 coatings deposited by high power impulse

magnetron sputtering. Surface & Coatings Technology, v. 253, p. 115-122, Aug 2014. ISSN 0257-8972.

[11] ZHANG, C. et al. Advanced Nanocluster Ion Source Based on High-Power Impulse Magnetron Sputtering and Time-Resolved Measurements of Nanocluster Formation. Journal of Physical Chemistry A, v. 117, n. 40, p. 10211-10217, Oct 10 2013. ISSN 1089-5639.

[12] PELLEG, J. et al. Compositional and structural changes in TiB2 films induced by bias, in situ and post-deposition annealing, respectively. **Physica B-Condensed Matter,** v. 381, n. 1-2, p. 118-127, May 2006. ISSN 0921-4526.

[13] CHANG, C.-L. et al. Effect of duty cycles on the deposition and characteristics of high power impulse magnetron sputtering deposited TiN thin films. Surface & Coatings Technology, v. 259, p. 232-237, Nov 25 2014. ISSN 0257-8972.

[14] PELLEG, J. et al. REACTIVE-SPUTTER-DEPOSITED TIN FILMS ON GLASS SUBSTRATES. **Thin Solid Films,** v. 197, n. 1-2, p. 117-128, Mar 1991. ISSN 0040-6090.

[15] NOUVEAU, C. et al. Stress and structure profiles for chromium nitride coatings deposited by r.f. magnetron sputtering. Thin Solid Films, v. 398, p. 490-495, Nov 2001. ISSN 0040-6090.

[16] ANDERS, A. A structure zone diagram including plasma-based deposition and ion etching. Thin Solid Films, v. 518, n. 15, p. 4087-4090, May 2010. ISSN 0040-6090.

[17] GRECZYNSKI, G. et al. A review of metal-ion-flux-controlled growth of metastable TiAlN by HIPIMS/DCMS co-sputtering. Surface & Coatings Technology, v. 257, p. 15-25, Oct 2014. ISSN 0257-8972.

[18] LIN, J. et al. Effect of negative substrate bias voltage on the structure and properties of CrN films deposited by modulated pulsed power (MPP) magnetron sputtering. Journal of Physics D-

Applied Physics, v. 44, n. 42, Oct 2011. ISSN 0022-3727. Disponível em: < <Go to ISI>://WOS:000296590300015 >.

[19] MACHUNZE, R.; EHIASARIAN, A.P.; TICHELAAR, F.D.; JANSSEN, G.C.A.M. Stress and texture in HIPIMS TiN thin films. Thin Solid Films, v. 518, p. 1561 – 1565, Sep 2009.

[20] CHIPATECUA, Y.L., OLAYA, J.J., ARIAS, D.F. Corrosion behaviour of CrN/Cr multilayers on stainless steel deposited by unbalanced magnetron sputtering. Vacuum, v. 86, p. 1393-1401, Mar. 14 2012. ISSN 0042-207X.

[21] X. GUAN, et. al. Microstructures and properties of Zr/CrN multilayer coatings fabricated by multi-arc ion plating. Tribology International, v. 106, p. 78-87, Feb 2017. ISSN 0301-679X.

[22] KAMBOJ, A., RAGHUPATHY, Y., REKHA, M.Y., SRIVASTAVA, C. Morphology, Texture and Corrosion Behavior of Nanocrystalline Copper–Graphene Composite Coatings. JOM. v. 69, p. 1149-54, Jul. 2017. ISSN 1047-4838.

[23] OU, Y.X., et. al. Wear and corrosion resistance of CrN/TiN superlattice coatings deposited by a combined deep oscillation magnetron sputtering and pulsed dc magnetron sputtering. Applied Surface Science, v.351, p. 332-43, Oct. 2015. ISSN 0169-4332.

[24] HOVSEPIAN, P.E., LEWIS, D.B., MÜNZ, W.D. Recent progress in large scale manufacturing of multilayer/superlattice hard coatings. Surface and Coatings Technology, v. 133, p. 166-75, Nov. 2000. ISSN 0257-8972.